Cell Reports

Oxygen-Sensitive Remodeling of Central Carbon Metabolism by Archaic eIF5B

Graphical Abstract

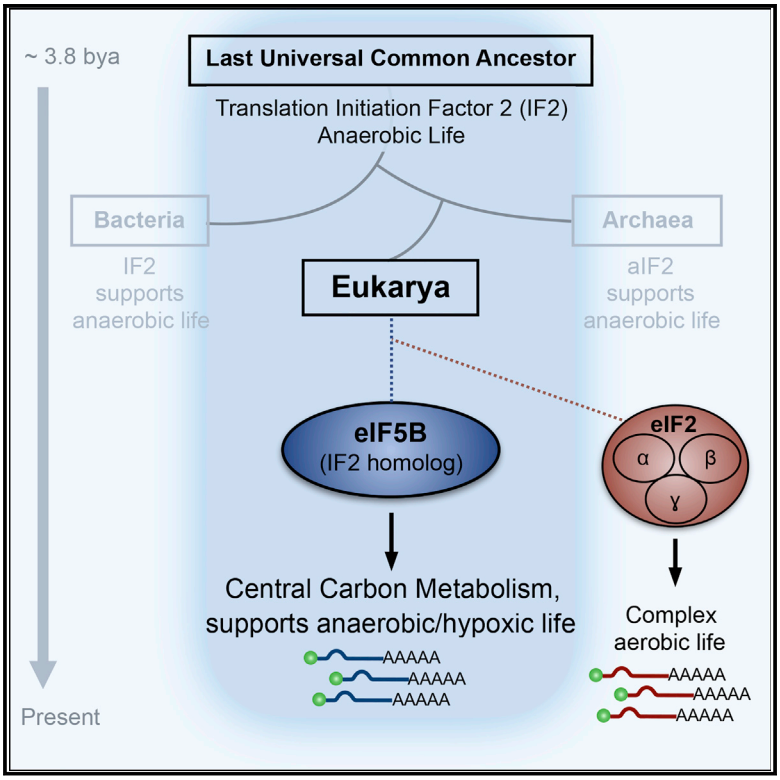

Highlights

- MATRIX produces system-wide blueprints of active translation factors
- eIF5B is an essential component of the hypoxic protein synthesis machinery
- eIF5B is the hypoxic surrogate of eIF2 that facilitates met-tRNAi^{Met} delivery
- Central carbon metabolism proteins are principally reliant on eIF5B for translation

Authors

J.J. David Ho, Nathan C. Balukoff, Grissel Cervantes, Petrice D. Malcolm, Jonathan R. Krieger, Stephen Lee

Correspondence

stephenlee@med.miami.edu

In Brief

Ho et al. employed MATRIX to demonstrate that eIF5B is an essential hypoxic translation factor that facilitates met-tRNAi^{Met} delivery to ribosomes, serving as the hypoxic surrogate of the textbook eIF2. Aerobic eukarya likely retained eIF5B for the oxygen-dependent regulation of central carbon metabolism and hypoxic survival.

Data and Software Availability

PXD006799

Ho et al., 2018, Cell Reports *22*, 17–26
January 2, 2018
https://doi.org/10.1016/j.celrep.2017.12.031

CellPress

Cell Reports
Report

Oxygen-Sensitive Remodeling of Central Carbon Metabolism by Archaic eIF5B

J.J. David Ho,[1,2] Nathan C. Balukoff,[1,2] Grissel Cervantes,[1,2] Petrice D. Malcolm,[1,2] Jonathan R. Krieger,[3] and Stephen Lee[1,2,4,5,*]

[1]Department of Biochemistry and Molecular Biology, Miller School of Medicine, University of Miami, Miami, FL 33136, USA
[2]Sylvester Comprehensive Cancer Center, Miller School of Medicine, University of Miami, Miami, FL 33136, USA
[3]The SickKids Proteomics, Analytics, Robotics & Chemical Biology Centre (SPARC BioCentre), The Hospital for Sick Children, Toronto, ON M5G 1X8, Canada
[4]Department of Urology, Miller School of Medicine, University of Miami, Miami, FL 33136, USA
[5]Lead Contact
*Correspondence: stephenlee@med.miami.edu
https://doi.org/10.1016/j.celrep.2017.12.031

SUMMARY

The eukaryotic translation initiation factor 5B (eIF5B) is a homolog of IF2, an ancient translation factor that enables initiator methionine-tRNAi^{Met} (met-tRNAi^{Met}) loading on prokaryotic ribosomes. While it can be traced back to the last universal common ancestor, eIF5B is curiously dispensable in modern aerobic yeast and mammalian cells. Here, we show that eIF5B is an essential element of the cellular hypoxic cap-dependent protein synthesis machinery. System-wide interrogation of dynamic translation machineries by MATRIX (mass spectrometry analysis of active translation factors using ribosome density fractionation and isotopic labeling experiments) demonstrated augmented eIF5B activity in hypoxic translating ribosomes. Global translatome studies revealed central carbon metabolism, cellular hypoxic adaptation, and ATF4-mediated stress response as major eIF5B-dependent pathways. These primordial processes rely on eIF5B even in the presence of oxygen and active eIF2, the canonical recruiter of met-tRNAi^{Met} in eukaryotes. We suggest that aerobic eukarya retained eIF5B/IF2 to remodel anaerobic pathways during episodes of oxygen deficiency.

INTRODUCTION

The first living cells appeared on Earth ~4 billion years ago in an oxygen-deficient environment (Weiss et al., 2016). To sustain anaerobic life, primeval cells generated energy (ATP) through early forms of glycolysis, a highly conserved core component of central carbon metabolism that exists in virtually all extant species (Koonin, 2003). The polypeptides required to catalyze these primordial metabolic reactions were synthesized by two core ancient translation factors: initiation factor 1 (IF1) and IF2 (Koonin, 2003). After ~1.5 billion years of anaerobic evolution, the increase in atmospheric oxygen catalyzed an upsurge in cellular energy production and biochemical complexity exemplified by contemporary eukaryotes (Falkowski, 2006; Raymond and Segrè, 2006). The eukaryotic protein synthesis machinery is a paragon of this expansion of complexity. For initiation alone, eukaryotic cells employ at least 13 core eukaryotic-specific translation initiation factors (eIFs) composed of 33 known subunits (Jackson et al., 2010), highlighting the significance of aerobic protein synthesis to modern eukaryotic life. Yet the ancestral IF2, which can be traced back to the last universal common ancestor (LUCA), remains conserved in eukaryotes as eIF5B (Choi et al., 1998; Lee et al., 1999), just as it is in bacteria (IF2) and archaea (aIF2) (Dever, 2002). Despite such strong evolutionary conservation, however, eIF5B is not essential in eukaryotes under basal conditions, exhibiting minimal effects on global translation and cell viability (Choi et al., 1998; Thakor and Holcik, 2012). These observations raise the intriguing possibility that eIF5B/IF2, which first evolved in the absence of oxygen, was retained during aerobic eukaryotic evolution as a mechanism to sustain protein synthesis during oxygen deficiency.

In prokaryotes, IF2 facilitates initiator formylated met-tRNA^{fMet} delivery to ribosomes (Laursen et al., 2005; Yatime et al., 2004). In contrast, this task is typically accomplished in eukaryotes by the textbook eIF2 that delivers met-tRNAi^{Met} to the 40S ribosomal subunit (Jackson et al., 2010; Sonenberg and Hinnebusch, 2009). eIF2 function is tightly regulated by the integrated stress response (ISR), a ubiquitous eukaryotic program activated by various environmental stresses, including hypoxia (Harding et al., 2000a; Pakos-Zebrucka et al., 2016; Wouters and Koritzinsky, 2008). During hypoxic episodes, ISR-inducible kinases phosphorylate the eIF2α subunit and inhibit eIF2 activity (Liu et al., 2006). Although ISR-mediated eIF2 inhibition should theoretically abolish translation initiation, hypoxic cells are capable of engaging in robust cap-dependent protein synthesis by eIF4F^{H}, the functional counterpart of the normoxic eIF4F (Ho et al., 2016; Liu et al., 2006; Uniacke et al., 2012). These data suggest that another translation initiation factor may complement, or assist, in the delivery of met-tRNAi^{Met} for eIF4F^{H}-directed translation during periods of hypoxic eIF2 inactivation.

In this study, we report that hypoxic cells exhibit increased dependence on eIF5B/IF2 for translation initiation and cell survival, with central carbon metabolism (CCM) being a major eIF5B-dependent target. A number of these targets rely preferentially on eIF5B, regardless of eIF2 activity. We suggest that

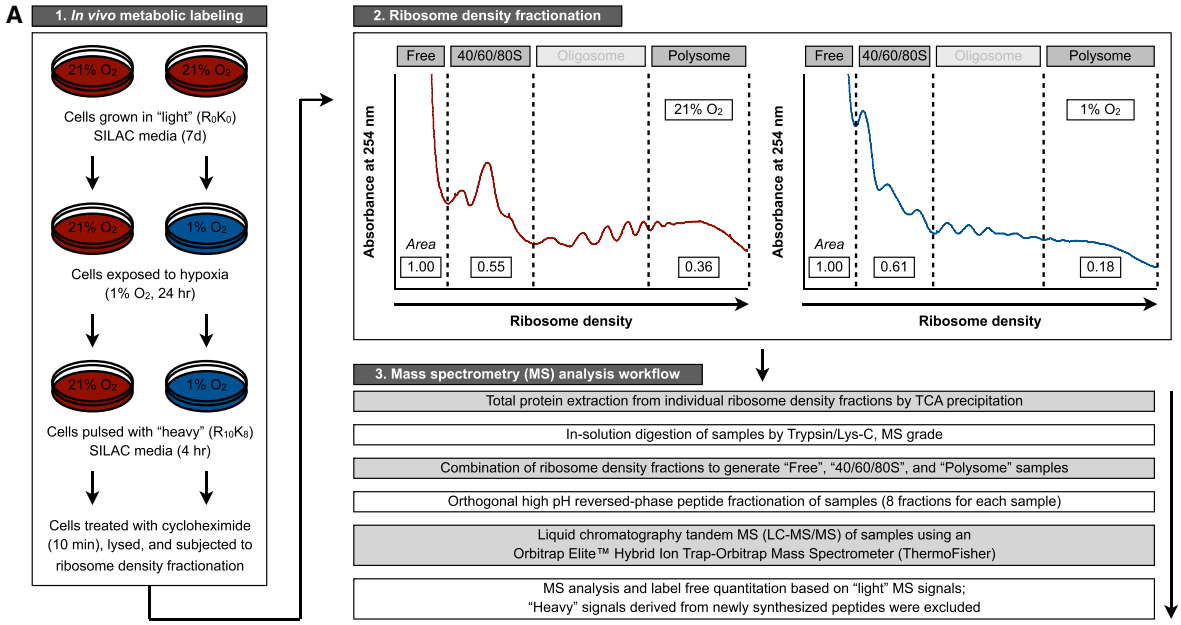

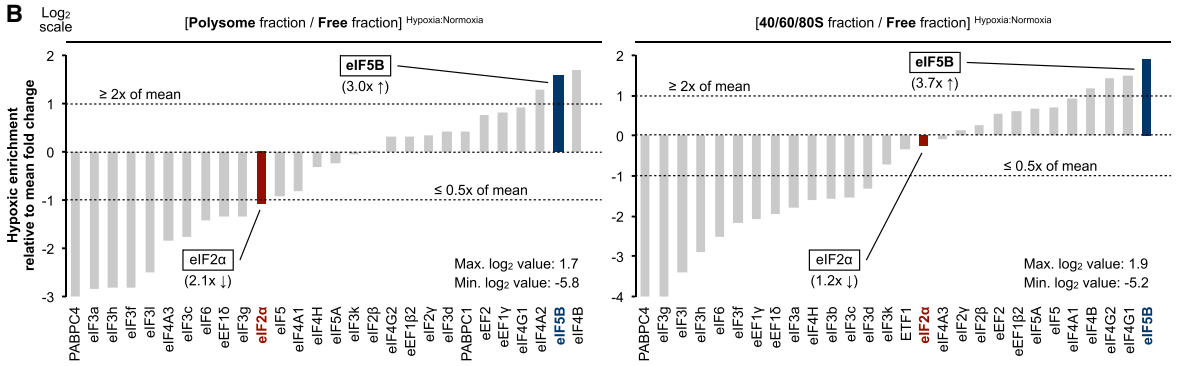

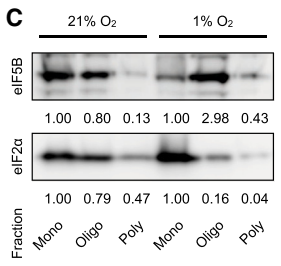

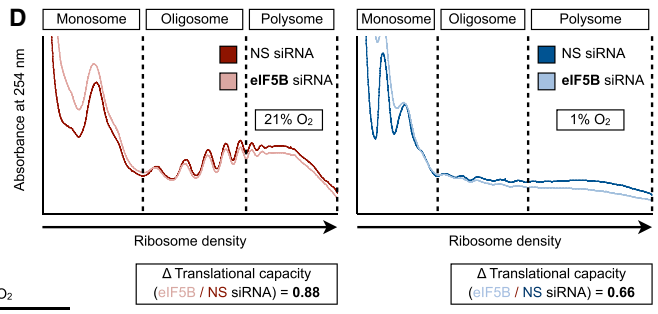

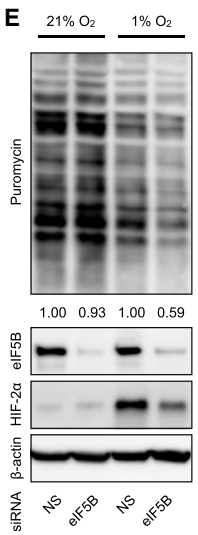

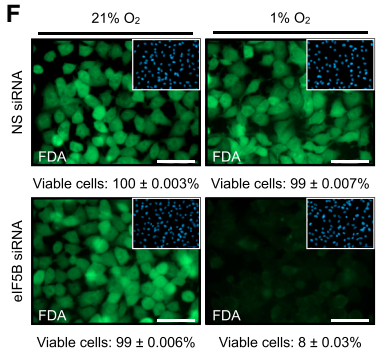

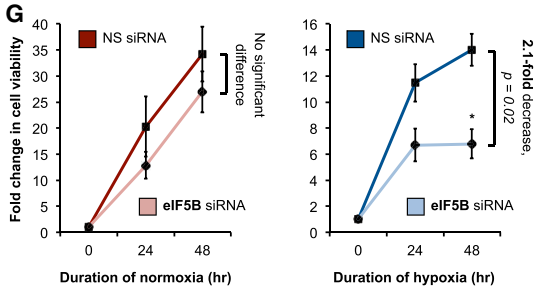

(legend on next page)

during aerobic eukaryotic evolution, metabolic pathways that first evolved under anaerobic conditions retained their reliance on eIF5B/IF2, which remains active during oxygen deprivation.

RESULTS

MATRIX Identifies eIF5B as a Hypoxia-Enriched Translation Factor

The ancient eIF5B/IF2 likely evolved in an anaerobic environment. We hypothesized that eIF5B retains the ability to operate in eukaryotic cells exposed to low oxygen (Figure S1A), a stress that inactivates the canonical eIF2. To test this hypothesis impartially, we developed a method to assess global translation factor activity in living cells, termed MATRIX (mass spectrometry analysis of active translation factors using ribosome density fractionation and isotopic labeling experiments) (Figure 1A). Integrating metabolic pulse labeling, ribosome density fractionation, and high-throughput mass spectrometry, MATRIX offers the capability to generate an architectural blueprint of biologically active cellular translational machineries. Ribosome density fractionation effectively separates cellular assets based on translational activity. Specifically, factors actively engaged in protein synthesis are preferentially enriched in polysome fractions, while those disengaged from active translation are relatively consigned to the free fractions. We also analyzed ribosomal 40/60/80S fractions, which allow us to assess factors involved in translation initiation more specifically. Oligosome (mild translation) fractions were excluded from analysis because of the ambiguous or transitional state of protein synthesis that they represent. To minimize the confounding presence of newly synthesized peptides and proteins, cells grown in light stable isotope labeling by amino acids in cell culture (SILAC) media were pulsed with heavy SILAC media before protein harvest. This allows us to identify and exclude from further analysis peptides derived from ongoing translation.

We performed MATRIX on U87MG glioblastoma cells subjected to normoxia (21% O_2) and hypoxia (1% O_2), a concentration that simultaneously activates eIF4F^H and inhibits eIF4F (Figure 1B) (Ho et al., 2016; Uniacke et al., 2012). The ratio of peptide/protein abundance in polysome fractions (active, intense translation) to free fractions (translationally disengaged) was used as the primary readout (Figure 1B, left panel). The abundance ratio of proteins engaged in translation initiation (40/60/80S fractions) to free fractions served as a secondary readout (Figure 1B, right panel). Overall, MATRIX detected 2,728 well-represented ($\geq$5 unique peptides) cellular factors (Table S1). We identified 30 translation factors with high confidence (i.e., detected across all measured fractions, $\geq$25% protein coverage). Based on the previously mentioned readouts, and an enrichment criterion of $\geq$2× mean fold change after outlier removal, MATRIX identified eIF5B (3× enrichment) (Figure 1B, blue highlight) as one of two translation factors (the other being eIF4B) that exhibited augmented activity under hypoxic conditions. Reassuringly, this impartial analysis confirmed the well-established hypoxic inhibition of eIF2α activity (2× decrease) (Figure 1B, red highlight). These findings were validated by immunoblot analysis of ribosome density fractions (Figure 1C). Thus, MATRIX analysis revealed that eIF5B concentrates in hypoxic translating ribosomes.

Involvement of eIF5B in Hypoxic Protein Synthesis

Next, we examined the effect of eIF5B depletion on global protein synthesis in various human cell lines exposed to normoxia or hypoxia using ribosome density profiling (Figures 1D and S1B). Normoxic eIF5B-depleted cells exhibited a modified ribosome density profile but maintained a largely similar translational intensity, as determined by quantitative area under curve measurements (Figures 1D, left panel, and S1C, top panel). In contrast, eIF5B-silencing in hypoxic cells resulted in a ~35% loss in translating ribosomes and decreased translational capacity (Figures 1D, right panel, and S1C, bottom panel). Similarly, puromycin incorporation showed that eIF5B silencing produced little discernable effect on normoxic translational capacity across multiple cell lines, while global translation was reproducibly decreased by ~40% in eIF5B-depleted hypoxic cells (Figures 1E and S1D). These findings agree with published observations that eIF5B is basally non-essential. Normoxic eIF5B depletion resulted only in a modest suppression of cell growth and viability (Figures 1F and 1G). In contrast, hypoxic cell viability was significantly decreased by eIF5B silencing (Figures 1F and 1G).

eIF5B Facilitates met-tRNAi^{Met} Delivery during Hypoxia

eIF2 is the paradigmatic translation initiation factor that delivers met-tRNAi^{Met} to eukaryotic ribosomes. As the affinity of eIF5B for met-tRNAi^{Met} is considerably lower than that of eIF2, several studies have suggested a role for this translation factor in 80S ribosomal subunit joining (Pestova et al., 2000; Terenin et al., 2008). Confirming the observation that eIF5B was functionally enriched in hypoxic translating ribosomes (Figure 1B), we observed increased association between eIF5B and tRNAi^{Met} in hypoxic versus normoxic conditions (Figures 2A and S2A). Likewise, eIF5B silencing caused a decrease in tRNAi^{Met} levels

Figure 1. MATRIX Identifies eIF5B as a Hypoxia-Enriched Translation Factor

(A) MATRIX workflow.

(B) MATRIX analysis of eukaryotic translation factor activity in hypoxic versus normoxic protein synthesis in U87MG. Ratios of peptide/protein abundance in polysome to free fractions (left panel) and 40/60/80S to free fractions (right panel) were calculated.

(C) MATRIX validation by immunoblot in normoxic and hypoxic U87MG. Representative immunoblots are shown. Mono, monosome (40/60/80S); oligo, oligosome; poly, polysome.

(D and E) Ribosome density profiling (D) and representative immunoblots (E) of normoxic and hypoxic U87MG treated with control non-silencing (NS) or eIF5B-specific small interfering RNA (siRNA).

(F and G) Fluorescein diacetate (FDA) staining (F, green) with DAPI counterstaining (F, inset, blue) and cell viability measurements (G) were performed in normoxic and hypoxic U87MG treated with NS or eIF5B-specific siRNA.

Error bars represent SEM. *$p < 0.05$. See also Figure S1.

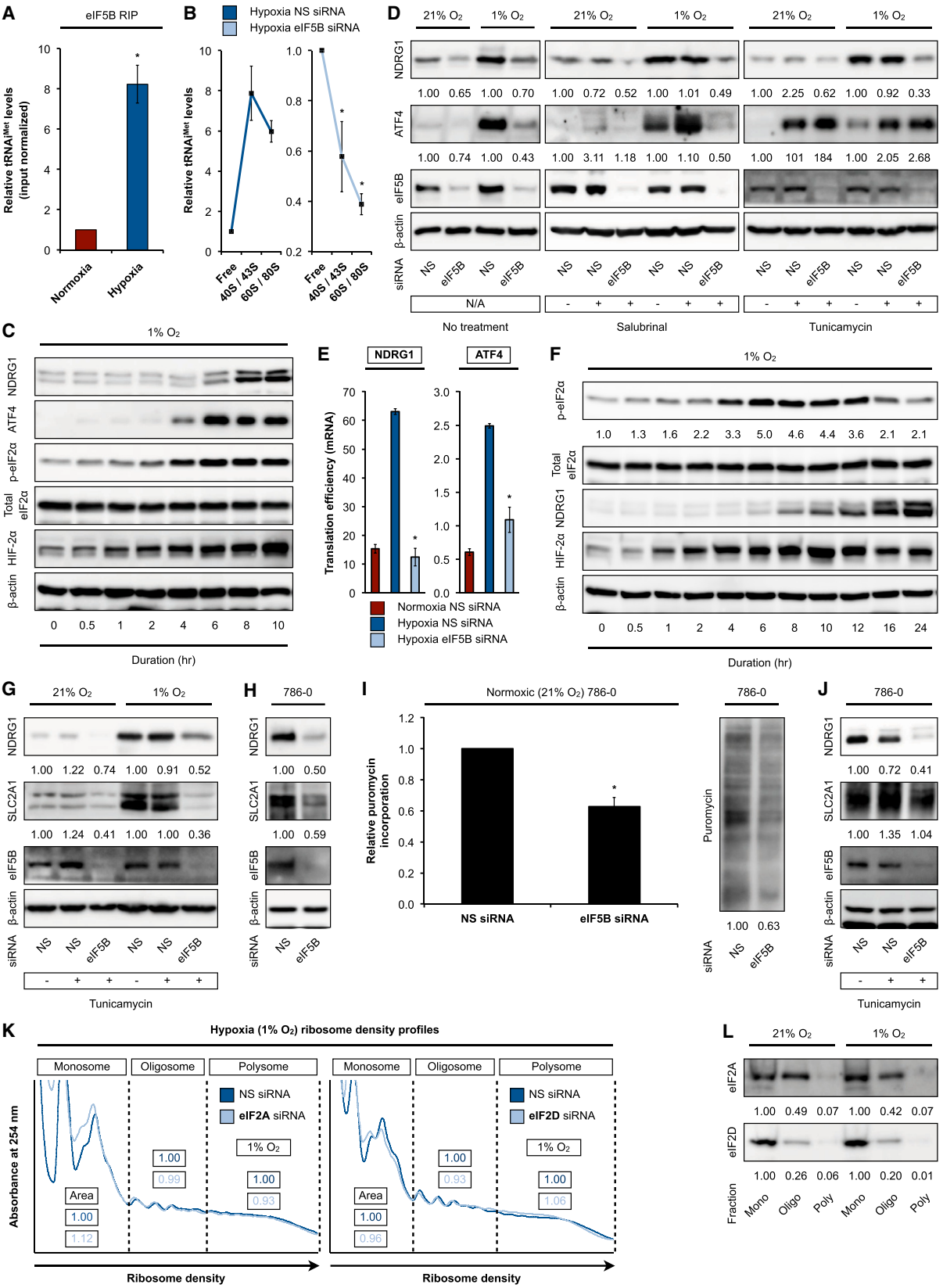

(legend on next page)

in hypoxic ribosomes compared to eIF5B-replete controls (Figure 2B), unlike elongating tRNAs, such as $tRNA^{Arg}$, which remained unaffected (Figure S2B). This hypoxic augmentation of eIF5B activity may be accounted for, at least partly, by increased met-$tRNAi^{Met}$ availability as a result of eIF2 inhibition. Hypoxia-induced eIF2α subunit phosphorylation and eIF2 inactivation correlate positively with the induction of both ATF4, a master transcription factor of ISR induced regardless of initiating stress (Pakos-Zebrucka et al., 2016), and NDRG1, a hypoxia-inducible protein (Ho et al., 2016) (Figure 2C). This suggested that the synthesis of hypoxia-inducible proteins is eIF2 independent, instead relying on alternative factors to deliver met-$tRNAi^{Met}$. eIF5B silencing severely attenuated the hypoxic induction of ATF4 and NDRG1 (Figures 2D and S2C, left panels) due to reduced translation efficiency (TE) (Figure 2E), but not steady-state levels of mRNAs (Figure S2D). Such hypoxic induction remained eIF5B dependent and eIF2 independent even following treatment with salubrinal, an ISR-prolonging eIF2 phosphatase inhibitor (Boyce et al., 2005) (Figures 2D and S2C, middle panels). Tunicamycin-induced endoplasmic reticulum (ER) stress, which leads to rapid eIF2α phosphorylation or eIF2 inactivation (Harding et al., 2000b), resulted in robust eIF5B-independent accumulation of the pan-stress-inducible ATF4, but not the hypoxia-induced protein NDRG1 (Figures 2D and S2C, right panels). Furthermore, cellular translational dependence on eIF5B was unaffected by heat shock (Figure S2E). These data suggested that eIF5B is preferentially regulated by hypoxic stress.

We next examined the relationship between eIF5B-dependent met-$tRNAi^{Met}$ delivery and eIF2 activity status. In certain cellular systems, prolonged hypoxia is associated with ISR recovery and eIF2 reactivation (via eIF2α dephosphorylation) (Figures 2F and S2F) (Koritzinsky et al., 2006). Yet the induction of classic hypoxia-inducible proteins, such as NDRG1 and glucose transporter GLUT1/SLC2A1, under prolonged hypoxia remained eIF5B dependent but eIF2 independent, even with tunicamycin- or salubrinal-induced augmentation of eIF2 inhibition (Figures 2G, S2G, and S2H). We were mindful of the possibility that residual eIF2α phosphorylation under prolonged hypoxia could preclude full reactivation of eIF2 activity (Figure 2F). To address this issue, we employed the 786-0 clear cell renal cell carcinoma cell model, which behaves as a pseudo-hypoxic system under basal, normoxic conditions due to the genetic loss of von Hippel-Lindau (VHL). As such, normoxic 786-0 engages simultaneously in both normoxic and hypoxic protein synthesis (Ho et al., 2016). This represents an ideal model system to examine basal, normoxic eIF2 and eIF5B activities without the need for hypoxic stimulation. Results indicated that eIF5B silencing markedly reduced eIF5B-dependent NDRG1 and GLUT1 protein levels (Figures 2H and S2I), as well as global protein synthesis in normoxic 786-0 (Figure 2I). Again, eIF5B-dependent targets demonstrated eIF2 independence even in normoxic 786-0 (Figures 2J and S2J). These data suggest that eIF5B may act as the hypoxic surrogate of eIF2 through direct met-$tRNAi^{Met}$ delivery to initiating ribosomes and/or through ribosomal subunit joining. The relative contributions of various eIF5B activities to its role in hypoxic translation, e.g., met-$tRNAi^{Met}$ recruitment, GTPase activity, and ribosomal subunit joining (Shin et al., 2002), remain to be determined in future studies. The translation factors eIF2A and eIF2D can assemble with met-$tRNAi^{Met}$ under specific conditions (Sendoel et al., 2017). However, eIF2A and eIF2D silencing did not significantly alter ribosome density profiles (Figures 2K and S2K) or global protein synthesis (Figure S2L), and we observed no accumulation of these factors in actively translating hypoxic ribosomes (Figure 2L).

Global Interrogation of eIF5B-Dependent Translatome Remodeling

Next, we sought to determine the eIF5B-dependent target population in hypoxic cells using an unbiased, integrative approach that combines high-throughput RNomic and proteomic analyses, enabling the assessment of steady-state RNA and protein levels and translational output (TE/protein output) from the same samples, respectively (Figure 3A). Consistent with our biochemical assays (Figures 1D and 1E), RNomic analysis revealed a global decrease in TE (Figure S3A) for more than 70% of detected mRNAs in eIF5B-depleted cells compared to controls (Figure 3B, top panel), with minimal correlation with RNA level changes (Figure 3B, bottom panel). The high sensitivity of this assay allowed us to detect many low-abundance mRNAs whose TE changes were likely masked by global-scale assessments (Figures 1D and 1E). Complementary to RNA-based translatome analysis (Floor and Doudna, 2016; Ho et al., 2016; Ingolia et al., 2009), live-cell metabolic labeling by pulse-SILAC (pSILAC)-mass spectrometry (MS) represents a reliable, direct readout for global

Figure 2. eIF5B Facilitates eIF2-Independent met-$tRNAi^{Met}$ Delivery

(A) eIF5B RNA immunoprecipitations (RIPs) followed by qRT-PCR measurements of input-normalized $tRNAi^{Met}$ levels from normoxic and hypoxic U87MG.

(B) Normoxic and hypoxic U87MG treated with control non-silencing (NS) or eIF5B-specific siRNA were subjected to ribosome density fractionation, followed by qRT-PCR measurements of $tRNAi^{Met}$ levels in the indicated fractions.

(C and D) Representative immunoblots of hypoxic U87MG (C) and normoxic and hypoxic (1% O_2, 10 hr) U87MG (D) treated with NS or eIF5B-specific siRNA (left panel) and with salubrinal (middle panel) or tunicamycin (right panel).

(E) Normoxic and hypoxic U87MG treated with NS or eIF5B-specific siRNA were subjected to ribosome density fractionation, followed by mRNA level measurements by qRT-PCR. Translation efficiency was defined as the ratio of polysome to monosome abundance.

(F–H) Representative immunoblots of hypoxic U87MG (F), normoxic and hypoxic U87MG treated with NS or eIF5B-specific siRNA and tunicamycin (G), and normoxic 786-0 treated with NS or eIF5B-specific siRNA (H).

(I) Puromycin incorporation measurements (left panel) and representative immunoblot (right panel) in normoxic 786-0 treated with NS or eIF5B-specific siRNA.

(J) Representative immunoblots of normoxic 786-0 treated with NS or eIF5B-specific siRNA and tunicamycin.

(K) Ribosome density profiling of hypoxic U87MG treated with NS, eIF2A-specific (left panel), or eIF2D-specific (right panel) siRNA. Area under curve measurements (area) are shown.

(L) Representative immunoblots of normoxic and hypoxic U87MG subjected to ribosome density fractionation.

Mono, monosome (40/60/80S); oligo, oligosome; poly, polysome. Error bars represent SEM. *$p < 0.05$. See also Figure S2.

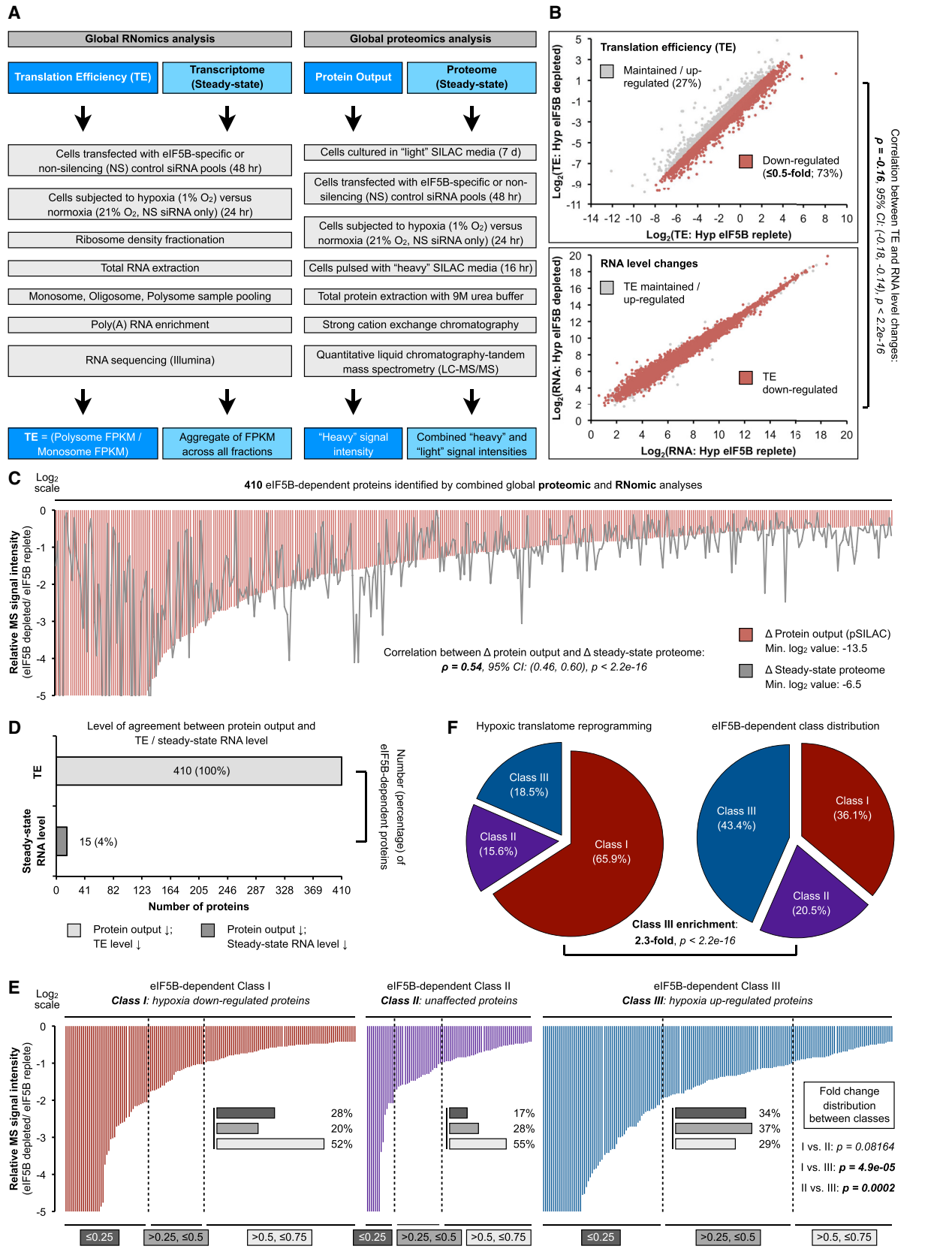

(legend on next page)

translational output (Schwanhäusser et al., 2011). Our pSILAC-MS analysis identified 480 proteins that exhibited reduced protein synthesis in eIF5B-depleted hypoxic cells (Figures 3C and S3B; Table S2). Translational output of these proteins exhibited significant positive correlation with steady-state protein levels (Figure 3C), and most (85%) demonstrated corresponding decreases in TE, but not RNA levels (Figures 3D and S3B).

We recently defined a class of eIF4F^{H}-dependent cellular mRNAs that are translationally enhanced under hypoxic conditions, termed class III (Ho et al., 2016). Class III members were more profoundly affected by eIF5B in terms of both magnitude (Figure 3E) and proportion (2× enrichment) (Figure 3F) compared to class I (translationally downregulated during hypoxia) and class II (translation unaffected by oxygen levels). Protein output in eIF5B-depleted cells showed significant positive correlation with steady-state protein levels across all three classes (Figure S3C). Altogether, these studies identified a sizable eIF5B-dependent target population and provide evidence for eIF5B as an essential component of the hypoxic protein synthesis machinery.

Central Carbon Metabolism Is a Major eIF5B-Dependent Target

Pathway enrichment analysis revealed the ancient pathways of central carbon metabolism and cellular hypoxic response as some of the most prominent eIF5B-dependent systems (Figures 4A, S4A, and S4B). Multi-dimensional validation confirms concordant changes in TE, protein output, and steady-state protein levels for each identified eIF5B target (Figures 4A, bottom panel; 4B; and S4B, bottom panel). The observation that most eIF5B-dependent proteins are class III members (Figure S4C) highlights the critical involvement of eIF5B in adaptive hypoxic translatome reprogramming. The number of eIF5B-dependent enzymes and proteins involved in central carbon metabolism and fructolysis demonstrates the vital eIF5B dependence of these pathways (Figures 4C and S4D). Unlike proteins involved in hypoxic adaptation (Figure 4D), proteins implicated in other cellular stresses, e.g., heat shock (Hsp27, Hsp70, and Hsp90), appear to be eIF5B independent, at least in our system (Figures S4E–S4G). In addition, hypoxia-inducible factor (HIF) alpha subunits HIF-1α and HIF-2α, which orchestrate the transcriptional (Wang et al., 1995) and translational (Uniacke et al., 2012) arms of the conserved cellular hypoxic response, exhibited notable eIF5B dependence (Figures 1E, 4A, 4D, S1D, S2C, and S2E–S2G). These findings underscore the unique role of eIF5B in hypoxic adaptation. Central carbon metabolism is a vital pathway that operates at a minimal basal level under normoxic conditions. Quantification of normoxic immunoblots revealed the eIF5B dependence of these pathways (e.g., GLUT1 and NDRG1) even under standard, normoxic conditions (Figures 2D and 2G), including in normoxic 786-0 (Figures 2H and 2J). Finally, we confirmed the normoxic dependence of central carbon metabolism on eIF5B using a global pSILAC assessment of protein output in eIF5B-depleted, normoxic 786-0 (Figure 4E).

DISCUSSION

In this report, we provide evidence that eIF5B is a key element of the cellular hypoxic protein synthesis machinery. Systemic translatome analyses revealed that eIF5B is principally involved in the translation of proteins involved in the ancient central carbon metabolism and cellular hypoxic response pathways. In addition, eIF5B is required for hypoxic cells to mount an ATF4-mediated stress response. It is tempting to speculate that eIF5B/IF2 was retained throughout the aerobic eukaryotic lineage to synthesize proteins that ensure cellular survival in oxygen-deficient environments, thus explaining their conservation to LUCA and across all domains of life. In addition, translatome analysis suggests that the HIF-2α and eIF4F^{H}-dependent class III mRNAs (Ho et al., 2016; Uniacke et al., 2012) rely mostly on eIF5B, even when eIF2 is active. These data suggest that eIF5B facilitates met-tRNAi^{Met} delivery for eIF4F^{H}-mediated hypoxic cap-dependent translation.

From a broader perspective, our findings provide further evidence for the emerging paradigm of alternative, stress-specific translation machineries, such as the hypoxic cap-binding complex eIF4F^{H} (Ho and Lee, 2016; Ho et al., 2016; Landon et al., 2014; Uniacke et al., 2012). Our current study expands upon this concept by demonstrating the hypoxic activation of eIF5B that may operate like eIF2A under certain eIF2-inactivating conditions (Sendoel et al., 2017).

Hypoxic augmentation of eIF5B activity was revealed by MATRIX, a global, unbiased approach that we developed to assess translation factor usage in living cells. Biological activity is a cornerstone of MATRIX, which prioritizes the ability to distinguish actively engaged translation factors from their disengaged or underused counterparts, especially across conditions. This feature offers MATRIX the innovative capability to reveal the lineup of active translation factors. This contrasts with studies that provide the roster or catalog of cellular factors, such as RNA-binding proteins (Castello et al., 2016) and ribosome-associated proteins (Simsek et al., 2017). Synergistic utilization of these complementary approaches could yield deeper insight into fundamental cellular processes, such as translation. We focused our current MATRIX analysis on known translation factors. Beyond these, MATRIX identified >70 ribosomal proteins, >40 recognized RNA-binding proteins, and many additional factors. Future studies are required to examine the biological roles of these factors.

Figure 3. Global Interrogation of eIF5B-Dependent Targets

(A) Workflow of RNomic and proteomic analyses.

(B) RNomic analysis of translation efficiency (TE) and steady-state RNA levels. Transcripts exhibiting decreased TE ($\leq$0.5-fold) are highlighted in red.

(C) eIF5B-dependent targets that exhibit decreased TE, protein output, and steady-state protein levels ($\leq$0.75-fold).

(D) Agreement between TE, steady-state RNA level and protein output.

(E) Effect of eIF5B depletion on magnitude of TE decrease across hypoxia-responsive mRNA classes.

(F) Proportions of the three hypoxia-responsive mRNA classes under eIF5B-replete and eIF5B-depleted (by siRNA) conditions.

See also Figure S3.

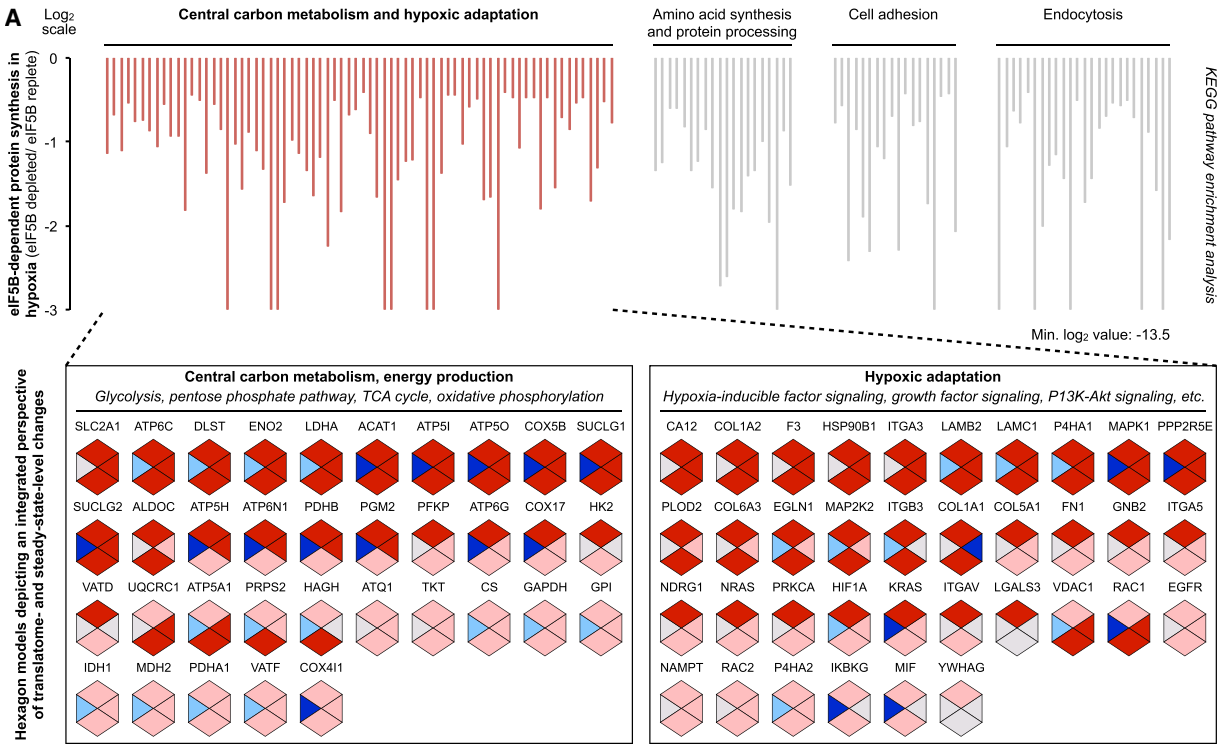

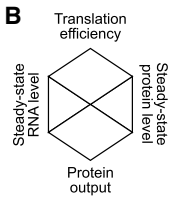

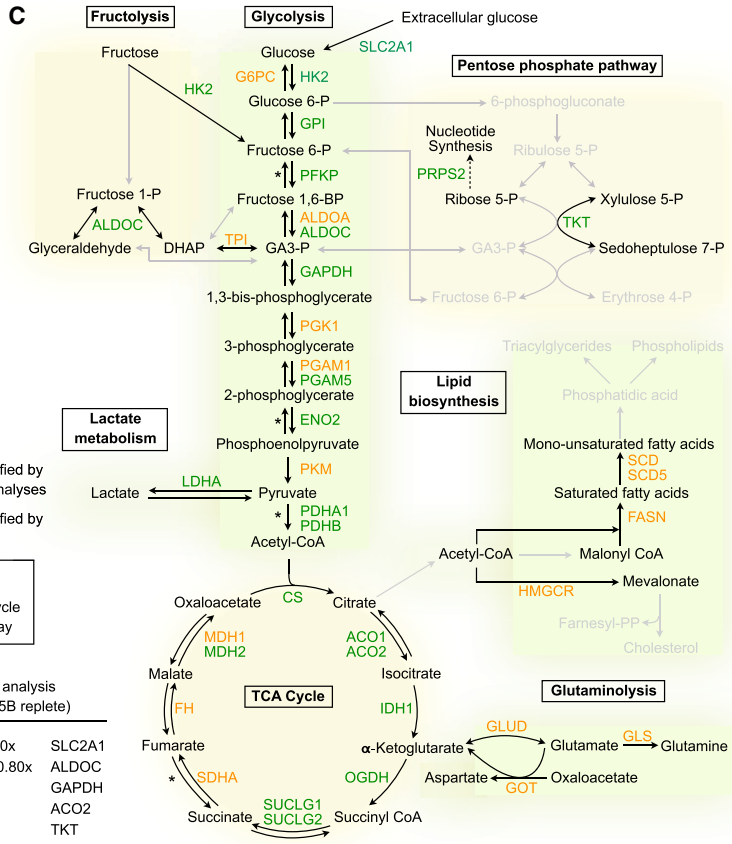

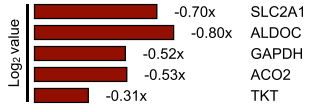

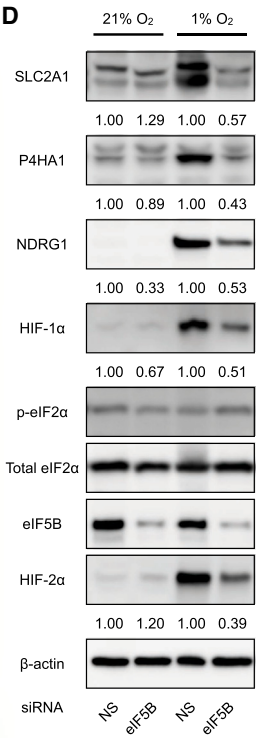

(legend on next page)

Our studies demonstrate that central carbon metabolism is intricately dependent on eIF5B during normoxia and especially hypoxia. Oxygen-dependent oxidative phosphorylation is the primary mechanism of cellular energy generation in aerobic eukaryotes. Because hypoxia inhibits this process, hypoxic cells engage in a complex, coordinated effort to augment central carbon metabolism (glucose intake, glycolysis, and trichloroacetic acid [TCA] cycle) to meet energy demands. In contrast, basal central carbon metabolism functions at a lower level under standard, normoxic conditions. This difference in central carbon metabolism activity or requirement may explain the increased eIF5B dependence of translation initiation and cell viability during hypoxia, as well as the non-essentiality of eIF5B under basal normoxic conditions (Choi et al., 1998; Thakor and Holcik, 2012). Our data suggest that eIF5B enables the hypoxia-induced glycolytic switch (Nakazawa et al., 2016). Therapeutically, enhancing normoxic eIF5B activity to augment aerobic glycolysis may benefit Leigh syndrome patients who suffer from defective oxidative phosphorylation. Conversely, eIF5B inhibition represents a potential anti-cancer therapy given that aerobic glycolysis, or the Warburg effect, is a hallmark of cancer (Hanahan and Weinberg, 2011).

Finally, there exist eukaryotic species that can subsist in low-oxygen conditions, e.g., naked mole rats (Park et al., 2017) and humans living at high altitude (e.g., Tibetan highlanders) (Yi et al., 2010). It will be interesting to determine in future studies any differences in eIF5B dependence or utilization between hypoxia-tolerant and hypoxia-intolerant species and/or populations.

EXPERIMENTAL PROCEDURES

Cell Culture and Reagents

U87MG, MCF7, and A549 cells were obtained from ATCC and propagated in DMEM (HyClone) with 10% fetal bovine serum (FBS) (Omega Scientific) and 1% penicillin-streptomycin (Pen-Strep) (HyClone). Cells were maintained at 37°C in a 5% CO_2 humidified incubator. Cells were subjected to hypoxia (1% O_2, 24 hr unless otherwise stated) at 37°C in a 5% CO_2, N_2-balanced, humidified H35 HypOxystation (HypOxygen). Final treatment concentrations were cycloheximide (Amresco) at 0.2 mg/mL, 75 μM salubrinal (Sigma-Aldrich) for 4 hr, and 25 μM tunicamycin (Sigma-Aldrich) for 4 hr.

SILAC

Cells were grown in light (R_0K_0) SILAC media (AthenaES) for 7 days before treatment. For MATRIX analysis, cells were pulsed with heavy ($R_{10}K_8$) SILAC media (AthenaES) for 4 hr (MATRIX) or 16 hr (pSILAC) following treatment.

Ribosome Density Fractionation

Polyribosome fractionations were performed essentially as previously described (Ho et al., 2016). Samples loaded based on equal cell number or equal total RNA yielded similar results. Total RNA was isolated from each fraction by phenol or chloroform extraction and ethanol precipitation following proteinase K treatment. Total protein was isolated by TCA precipitation.

MS Analysis

Liquid chromatography-tandem MS was performed by the SPARC BioCentre (The Hospital for Sick Children, Toronto, Canada). More details are provided in Supplemental Information.

RNA Sequencing Analysis

Poly(A) RNA selection was performed before library preparation and RNA sequencing runs. More details are provided in Supplemental Information.

Statistical Analysis

All experiments were performed at least three independent times, unless otherwise stated. Appropriate statistical analyses were performed, including Student's t tests, Pearson's correlation coefficient (ρ) calculations with 95% confidence intervals and p values, and chi-square tests, to investigate proportional differences. Statistical significance was defined as $p < 0.05$.

DATA AND SOFTWARE AVAILABILITY

The accession number for the MS datasets reported in this paper is ProteomeXchange: PXD006799. The accession number for the RNA sequencing datasets reported in this paper is SRA: SRP110475.

SUPPLEMENTAL INFORMATION

Supplemental Information includes Supplemental Experimental Procedures, four figures, and two tables and can be found with this article online at https://doi.org/10.1016/j.celrep.2017.12.031.

ACKNOWLEDGMENTS

S.L. is funded by grants from the NIH (NIGMS, 1R01GM115342, and NCI, 1R01CA200676) and the Sylvester Comprehensive Cancer Center. J.J.D.H. is a recipient of a Canadian Institutes of Health Research (CIHR) Postdoctoral Fellowship. We thank Dr. Siôn Ll. Williams and Dr. Steven Chen from the Sylvester Comprehensive Cancer Center Oncogenomics Core Facility and Biostatistics and Bioinformatics Core Facility, respectively, for RNA sequencing and analysis services.

AUTHOR CONTRIBUTIONS

J.J.D.H. and S.L. conceptualized the study and MATRIX. J.J.D.H. and S.L. conceived the experiments. J.J.D.H., N.C.B., G.C., P.D.M., and J.R.K. performed the experiments. J.J.D.H., N.C.B., J.R.K., and S.L. analyzed the data. J.J.D.H. and S.L. wrote the manuscript.

DECLARATION OF INTERESTS

The authors declare no competing interests.

Figure 4. Central Carbon Metabolism Is a Major eIF5B-Dependent Pathway

(A) Kyoto Encyclopedia of Genes and Genomes (KEGG) pathway enrichment analysis of eIF5B-dependent cellular processes (top panel). Hexagon models depicting TE, steady-state RNA level, protein output, and steady-state protein level for each identified protein involved in central carbon metabolism and hypoxic adaptation are shown (bottom panel).

(B) Legend for models in Figures 4A and S4A.

(C) eIF5B-dependent enzymes and proteins of central carbon metabolism and fructolysis identified by protein output and/or TE analyses. The asterisk indicates additional identified enzymes and/or isoforms (Figure S4D).

(D) Representative immunoblots of eIF5B-dependent proteins from normoxic and hypoxic U87MG treated with non-silencing (NS) control or eIF5B-specific siRNA.

(E) pSILAC analysis of protein output in normoxic 786-0 treated with NS or eIF5B-specific siRNA.

See also Figure S4.

Received: July 6, 2017
Revised: October 20, 2017
Accepted: December 8, 2017
Published: January 2, 2018

REFERENCES

Boyce, M., Bryant, K.F., Jousse, C., Long, K., Harding, H.P., Scheuner, D., Kaufman, R.J., Ma, D., Coen, D.M., Ron, D., and Yuan, J. (2005). A selective inhibitor of eIF2alpha dephosphorylation protects cells from ER stress. Science *307*, 935–939.

Castello, A., Fischer, B., Frese, C.K., Horos, R., Alleaume, A.M., Foehr, S., Curk, T., Krijgsveld, J., and Hentze, M.W. (2016). Comprehensive identification of RNA-binding domains in human cells. Mol. Cell *63*, 696–710.

Choi, S.K., Lee, J.H., Zoll, W.L., Merrick, W.C., and Dever, T.E. (1998). Promotion of met-tRNAiMet binding to ribosomes by yIF2, a bacterial IF2 homolog in yeast. Science *280*, 1757–1760.

Dever, T.E. (2002). Gene-specific regulation by general translation factors. Cell *108*, 545–556.

Falkowski, P.G. (2006). Evolution. Tracing oxygen's imprint on Earth's metabolic evolution. Science *311*, 1724–1725.

Floor, S.N., and Doudna, J.A. (2016). Tunable protein synthesis by transcript isoforms in human cells. eLife *5*, e10921.

Hanahan, D., and Weinberg, R.A. (2011). Hallmarks of cancer: the next generation. Cell *144*, 646–674.

Harding, H.P., Novoa, I., Zhang, Y., Zeng, H., Wek, R., Schapira, M., and Ron, D. (2000a). Regulated translation initiation controls stress-induced gene expression in mammalian cells. Mol. Cell *6*, 1099–1108.

Harding, H.P., Zhang, Y., Bertolotti, A., Zeng, H., and Ron, D. (2000b). Perk is essential for translational regulation and cell survival during the unfolded protein response. Mol. Cell *5*, 897–904.

Ho, J.J., and Lee, S. (2016). A cap for every occasion: alternative eIF4F complexes. Trends Biochem. Sci. *41*, 821–823.

Ho, J.J.D., Wang, M., Audas, T.E., Kwon, D., Carlsson, S.K., Timpano, S., Evagelou, S.L., Brothers, S., Gonzalgo, M.L., Krieger, J.R., et al. (2016). Systemic reprogramming of translation efficiencies on oxygen stimulus. Cell Rep. *14*, 1293–1300.

Ingolia, N.T., Ghaemmaghami, S., Newman, J.R., and Weissman, J.S. (2009). Genome-wide analysis in vivo of translation with nucleotide resolution using ribosome profiling. Science *324*, 218–223.

Jackson, R.J., Hellen, C.U., and Pestova, T.V. (2010). The mechanism of eukaryotic translation initiation and principles of its regulation. Nat. Rev. Mol. Cell Biol. *11*, 113–127.

Koonin, E.V. (2003). Comparative genomics, minimal gene-sets and the last universal common ancestor. Nat. Rev. Microbiol. *1*, 127–136.

Koritzinsky, M., Magagnin, M.G., van den Beucken, T., Seigneuric, R., Savelkouls, K., Dostie, J., Pyronnet, S., Kaufman, R.J., Weppler, S.A., Voncken, J.W., et al. (2006). Gene expression during acute and prolonged hypoxia is regulated by distinct mechanisms of translational control. EMBO J. *25*, 1114–1125.

Landon, A.L., Muniandy, P.A., Shetty, A.C., Lehrmann, E., Volpon, L., Houng, S., Zhang, Y., Dai, B., Peroutka, R., Mazan-Mamczarz, K., et al. (2014). MNKs act as a regulatory switch for eIF4E1 and eIF4E3 driven mRNA translation in DLBCL. Nat. Commun. *5*, 5413.

Laursen, B.S., Sørensen, H.P., Mortensen, K.K., and Sperling-Petersen, H.U. (2005). Initiation of protein synthesis in bacteria. Microbiol. Mol. Biol. Rev. *69*, 101–123.

Lee, J.H., Choi, S.K., Roll-Mecak, A., Burley, S.K., and Dever, T.E. (1999). Universal conservation in translation initiation revealed by human and archaeal homologs of bacterial translation initiation factor IF2. Proc. Natl. Acad. Sci. USA *96*, 4342–4347.

Liu, L., Cash, T.P., Jones, R.G., Keith, B., Thompson, C.B., and Simon, M.C. (2006). Hypoxia-induced energy stress regulates mRNA translation and cell growth. Mol. Cell *21*, 521–531.

Nakazawa, M.S., Keith, B., and Simon, M.C. (2016). Oxygen availability and metabolic adaptations. Nat. Rev. Cancer *16*, 663–673.

Pakos-Zebrucka, K., Koryga, I., Mnich, K., Ljujic, M., Samali, A., and Gorman, A.M. (2016). The integrated stress response. EMBO Rep. *17*, 1374–1395.

Park, T.J., Reznick, J., Peterson, B.L., Blass, G., Omerbašić, D., Bennett, N.C., Kuich, P.H.J.L., Zasada, C., Browe, B.M., Hamann, W., et al. (2017). Fructose-driven glycolysis supports anoxia resistance in the naked mole-rat. Science *356*, 307–311.

Pestova, T.V., Lomakin, I.B., Lee, J.H., Choi, S.K., Dever, T.E., and Hellen, C.U. (2000). The joining of ribosomal subunits in eukaryotes requires eIF5B. Nature *403*, 332–335.

Raymond, J., and Segrè, D. (2006). The effect of oxygen on biochemical networks and the evolution of complex life. Science *311*, 1764–1767.

Schwanhäusser, B., Busse, D., Li, N., Dittmar, G., Schuchhardt, J., Wolf, J., Chen, W., and Selbach, M. (2011). Global quantification of mammalian gene expression control. Nature *473*, 337–342.

Sendoel, A., Dunn, J.G., Rodriguez, E.H., Naik, S., Gomez, N.C., Hurwitz, B., Levorse, J., Dill, B.D., Schramek, D., Molina, H., et al. (2017). Translation from unconventional 5′ start sites drives tumour initiation. Nature *541*, 494–499.

Shin, B.S., Maag, D., Roll-Mecak, A., Arefin, M.S., Burley, S.K., Lorsch, J.R., and Dever, T.E. (2002). Uncoupling of initiation factor eIF5B/IF2 GTPase and translational activities by mutations that lower ribosome affinity. Cell *111*, 1015–1025.

Simsek, D., Tiu, G.C., Flynn, R.A., Byeon, G.W., Leppek, K., Xu, A.F., Chang, H.Y., and Barna, M. (2017). The mammalian ribo-interactome reveals ribosome functional diversity and heterogeneity. Cell *169*, 1051–1065.

Sonenberg, N., and Hinnebusch, A.G. (2009). Regulation of translation initiation in eukaryotes: mechanisms and biological targets. Cell *136*, 731–745.

Terenin, I.M., Dmitriev, S.E., Andreev, D.E., and Shatsky, I.N. (2008). Eukaryotic translation initiation machinery can operate in a bacterial-like mode without eIF2. Nat. Struct. Mol. Biol. *15*, 836–841.

Thakor, N., and Holcik, M. (2012). IRES-mediated translation of cellular messenger RNA operates in eIF2α-independent manner during stress. Nucleic Acids Res. *40*, 541–552.

Uniacke, J., Holterman, C.E., Lachance, G., Franovic, A., Jacob, M.D., Fabian, M.R., Payette, J., Holcik, M., Pause, A., and Lee, S. (2012). An oxygen-regulated switch in the protein synthesis machinery. Nature *486*, 126–129.

Wang, G.L., Jiang, B.H., Rue, E.A., and Semenza, G.L. (1995). Hypoxia-inducible factor 1 is a basic-helix-loop-helix-PAS heterodimer regulated by cellular O2 tension. Proc. Natl. Acad. Sci. USA *92*, 5510–5514.

Weiss, M.C., Sousa, F.L., Mrnjavac, N., Neukirchen, S., Roettger, M., Nelson-Sathi, S., and Martin, W.F. (2016). The physiology and habitat of the last universal common ancestor. Nat. Microbiol. *1*, 16116.

Wouters, B.G., and Koritzinsky, M. (2008). Hypoxia signalling through mTOR and the unfolded protein response in cancer. Nat. Rev. Cancer *8*, 851–864.

Yatime, L., Schmitt, E., Blanquet, S., and Mechulam, Y. (2004). Functional molecular mapping of archaeal translation initiation factor 2. J. Biol. Chem. *279*, 15984–15993.

Yi, X., Liang, Y., Huerta-Sanchez, E., Jin, X., Cuo, Z.X., Pool, J.E., Xu, X., Jiang, H., Vinckenbosch, N., Korneliussen, T.S., et al. (2010). Sequencing of 50 human exomes reveals adaptation to high altitude. Science *329*, 75–78.

Cell Reports, Volume *22*

Supplemental Information

Oxygen-Sensitive Remodeling of Central Carbon Metabolism by Archaic eIF5B

J.J. David Ho, Nathan C. Balukoff, Grissel Cervantes, Petrice D. Malcolm, Jonathan R. Krieger, and Stephen Lee

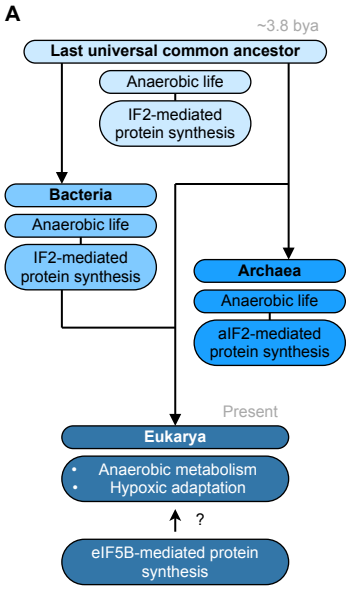

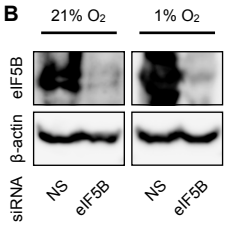

C **Relative areas under the curve for eIF5B knockdown ribosome density profiles**

21% O_2 - Area	Monosome	Oligosome	Polysome
NS siRNA	1.00	1.00	1.00
eIF5B siRNA	1.23	0.91	0.86
		Average = 0.88	

1% O_2 - Area	Monosome	Oligosome	Polysome
NS siRNA	1.00	1.00	1.00
eIF5B siRNA	1.10	**0.85**	**0.48**
		Average = **0.66**	

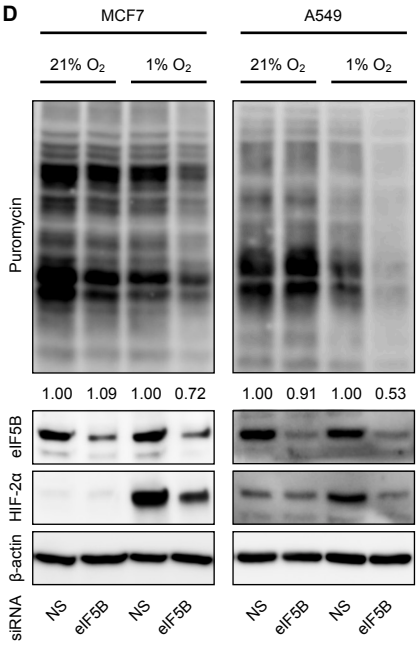

Figure S1. Related to Figure 1. (A) Model for the hypothesis that eIF5B was conserved throughout the evolution of aerobic eukaryotes for hypoxic adaptation and metabolism. IF2/eIF5B likely evolved in the last universal common ancestor under anaerobic conditions, and contemporary bacterial and archaeal IF2 homologs are capable of performing protein synthesis during oxygen deficiency. **(B)** Validation of siRNA-mediated eIF5B knockdown success by immunoblot for Figure 1D. Representative immunoblots are shown. **(C)** Area under curve measurements of ribosome density profiles of normoxic and hypoxic U87MG treated with control non-silencing (NS) or eIF5B-specific siRNA (Figure 1D). **(D)** Representative immunoblots of normoxic and hypoxic MCF7 and A549 treated with NS or eIF5B-specific siRNA.

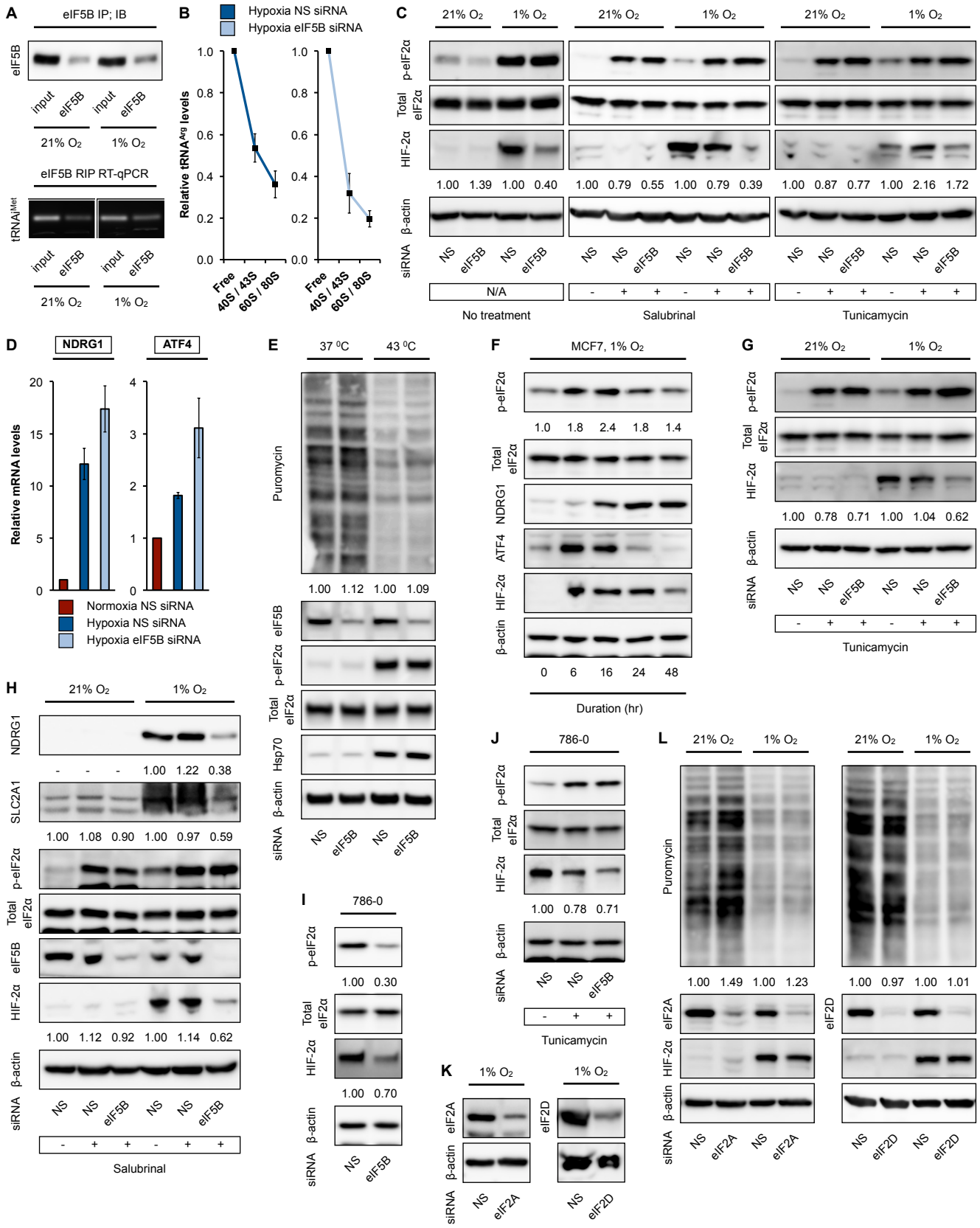
A
eIF5B IP; IB
eIF5B
input
eIF5B
input
eIF5B
21% O2
1% O2
eIF5B RIP RT-qPCR
tRNAiMet
input
eIF5B
input
eIF5B
21% O2
1% O2
B
Hypoxia NS siRNA
Hypoxia eIF5B siRNA
Relative tRNAArg levels
Free
40S / 43S
60S / 80S
Free
40S / 43S
60S / 80S
C
21% O2
1% O2
21% O2
1% O2
21% O2
1% O2
p-eIF2α
Total eIF2α
HIF-2α
1.00 1.39 1.00 0.40 1.00 0.79 0.55 1.00 0.79 0.39 1.00 0.87 0.77 1.00 2.16 1.72
β-actin
siRNA
NS
eIF5B
NS
eIF5B
NS
NS
eIF5B
NS
NS
eIF5B
NS
NS
eIF5B
NS
NS
eIF5B
N/A
- + + - + +
- + + - + +
No treatment
Salubrinal
Tunicamycin
D
NDRG1
ATF4
Relative mRNA levels
Normoxia NS siRNA
Hypoxia NS siRNA
Hypoxia eIF5B siRNA
E
37 °C
43 °C
Puromycin
1.00 1.12 1.00 1.09
eIF5B
p-eIF2α
Total eIF2α
Hsp70
β-actin
siRNA
NS
eIF5B
NS
eIF5B
F
MCF7, 1% O2
p-eIF2α
1.0 1.8 2.4 1.8 1.4
Total eIF2α
NDRG1
ATF4
HIF-2α
β-actin
0 6 16 24 48
Duration (hr)
G
21% O2
1% O2
p-eIF2α
Total eIF2α
HIF-2α
1.00 0.78 0.71 1.00 1.04 0.62
β-actin
siRNA
NS
NS
eIF5B
NS
NS
eIF5B
- + + - + +
Tunicamycin
H
21% O2
1% O2
NDRG1
- - - 1.00 1.22 0.38
SLC2A1
1.00 1.08 0.90 1.00 0.97 0.59
p-eIF2α
Total eIF2α
eIF5B
HIF-2α
1.00 1.12 0.92 1.00 1.14 0.62
β-actin
siRNA
NS
NS
eIF5B
NS
NS
eIF5B
- + + - + +
Salubrinal
I
786-0
p-eIF2α
1.00 0.30
Total eIF2α
HIF-2α
1.00 0.70
β-actin
siRNA
NS
eIF5B
J
786-0
p-eIF2α
Total eIF2α
HIF-2α
1.00 0.78 0.71
β-actin
siRNA
NS
NS
eIF5B
- + +
Tunicamycin
K
1% O2
1% O2
eIF2A
eIF2D
β-actin
siRNA
NS
eIF2A
NS
eIF2D
L
21% O2
1% O2
21% O2
1% O2
Puromycin
1.00 1.49 1.00 1.23
1.00 0.97 1.00 1.01
eIF2A
eIF2D
HIF-2α
β-actin
siRNA
NS
eIF2A
NS
eIF2A
NS
eIF2D
NS
eIF2D

Figure S2. Related to Figure 2. (A) Validation of eIF5B IP by immunoblot (top panel) and agarose gel images of RT-qPCR products after 40 amplification cycles (bottom panel) for Figure 2A. Representative images are shown. **(B)** Normoxic and hypoxic U87MG treated with control non-silencing (NS) or eIF5B-specific siRNA were subjected to ribosome density fractionation, followed by RT-qPCR measurements of elongator $tRNA^{Arg}$ levels in free, 40S/43S, and 60S/80S fractions. **(C)** Representative control immunoblots for Figure 2D. **(D)** Normoxic and hypoxic U87MG treated with control non-silencing (NS) or eIF5B-specific siRNA were subjected to ribosome density fractionation, followed by RT-qPCR measurements of NDRG1 and ATF4 steady-state mRNA levels (based on aggregate abundance across all fractions). **(E)** Representative immunoblots of U87MG exposed to 4 hr of heat shock (43 ^{0}C) versus untreated controls (37 ^{0}C). **(F)** Representative immunoblots of hypoxic (time course) MCF7. **(G)** Representative control immunoblots for Figure 2G. **(H)** Representative immunoblots of normoxic and hypoxic (24 hr) U87MG treated with NS or eIF5B-specific siRNA and salubrinal. **(I)** Representative control immunoblots for Figure 2H. **(J)** Representative control immunoblots for Figure 2J. **(K)** Validation of siRNA-mediated eIF2A and eIF2D knockdown success by immunoblot for Figure 2K. Representative immunoblots are shown. **(L)** Representative immunoblots of normoxic and hypoxic U87MG treated with NS, eIF2A-specific (left panel), or eIF2D-specific (right panel) siRNA.

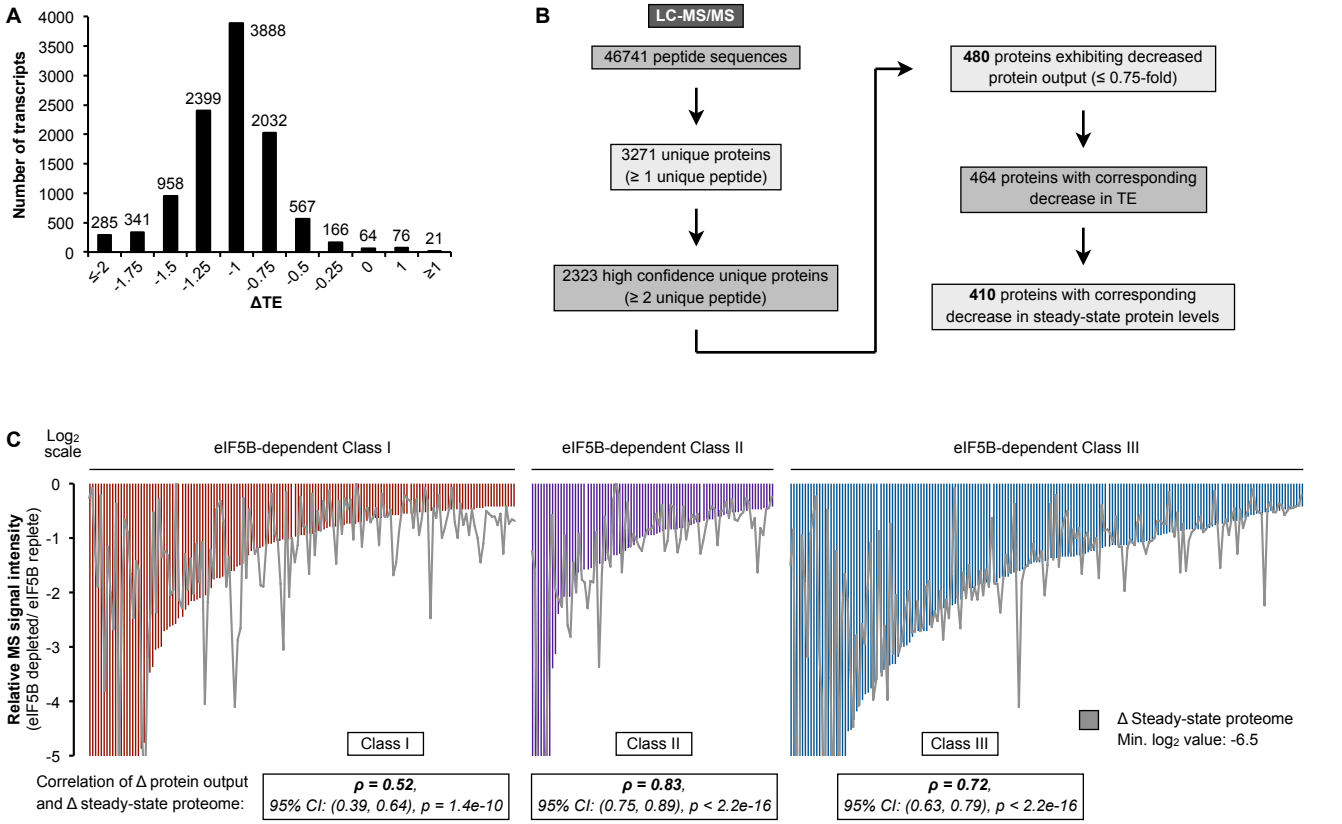

Figure S3. Related to Figure 3. (A) Transcript distribution profile of TE changes in eIF5B depleted (eIF5B-specific siRNA) versus eIF5B replete (control non-silencing (NS) siRNA), hypoxic U87MG cells. **(B)** Liquid chromatography tandem mass spectrometry (LC-MS/MS) analysis workflow for identifying eIF5B-dependent targets that show concordant changes in TE, protein output, and steady-state protein level. **(C)** Correlation between protein output and steady-state protein level for eIF5B-dependent targets classified based on hypoxia-responsiveness. Class I and III members are preferentially translated in normoxia and hypoxia, respectively, whereas Class II members are translated across oxygen levels.

A **KEGG pathway enrichment analysis of eIF5B-dependent targets**

KEGG pathway	*KEGG identifier term(s)*	*Lowest p value*	*Benjamini-corrected p value*	*Fold enrichment*
Carbon metabolism	hsa01200	1.80e-07	2.21e-05	4.20
Glycolysis	hsa00010	4.30e-04	8.11e-03	3.90
TCA cycle	hsa00020	1.89e-04	7.71e-03	6.33
Pentose phosphate pathway	hsa00030	6.52e-03	5.78e-02	4.91
Pyruvate metabolism	hsa00620	5.97e-03	5.51e-02	4.16
Oxidative phosphorylation	hsa00190	9.76e-03	7.27e-02	2.32
Hypoxic adaptation	hsa04066, hsa04151, hsa04370	2.55e-03	3.42e-03	2.91
Amino acid synthesis and protein processing	hsa01230, hsa04141	2.32e-04	6.32e-03	3.85
Cell adhesion	hsa04015, hsa04510, hsa04512, hsa04540	3.06e-06	2.51e-04	4.32
Endocytosis	hsa04144, hsa04145	1.91e-04	6.70e-03	2.30

B

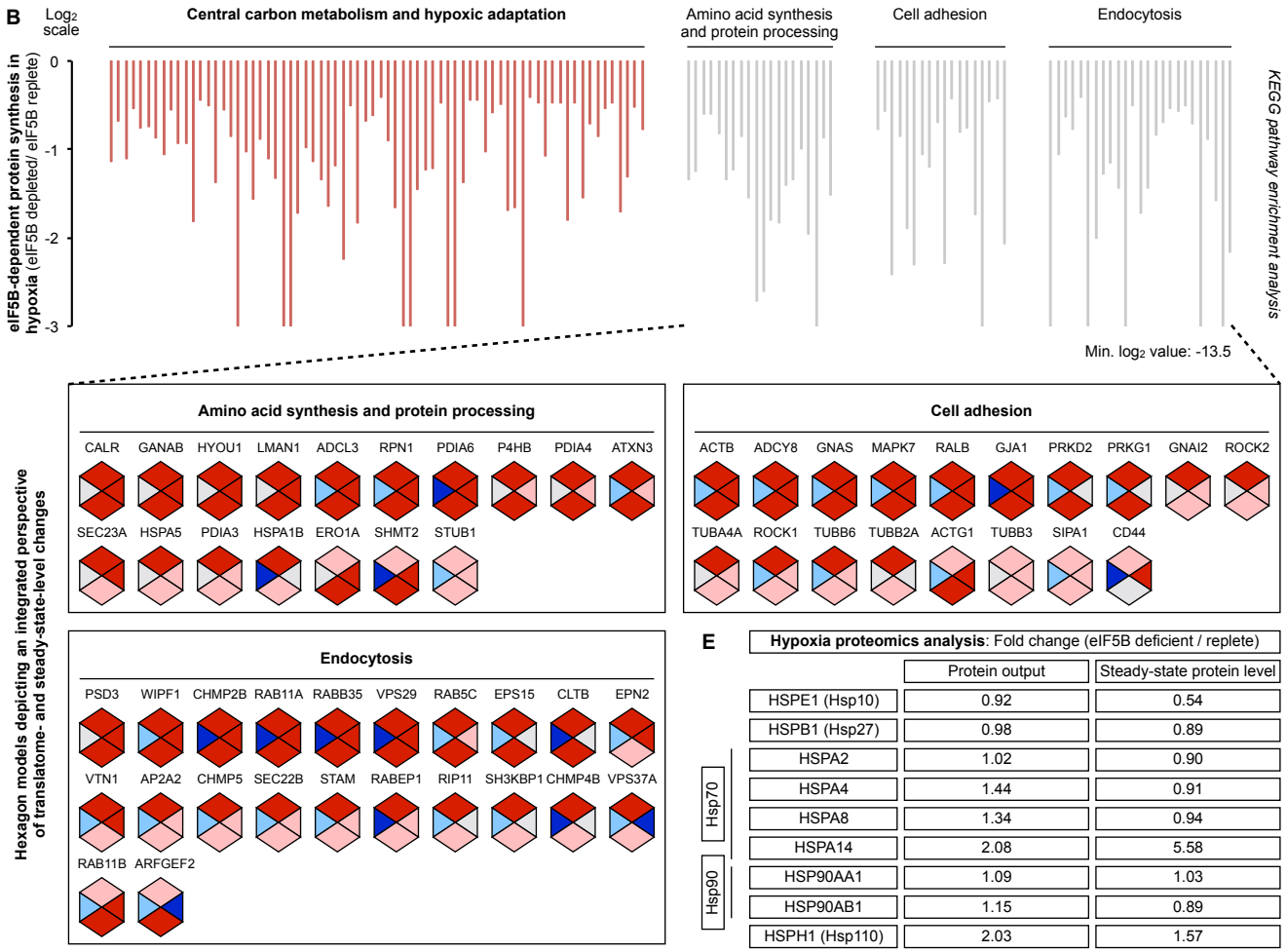

C

	Class I	Class II	**Class III**
Central carbon metabolism and hypoxic adaptation	15 (21%)	10 (14%)	47 (**65%**)
Amino acid synthesis and protein processing	4 (20%)	2 (10%)	14 (**70%**)
Cell adhesion	5 (27.7%)	3 (16.7%)	10 (**55.6%**)
Endocytosis	11 (44%)	4 (16%)	10 (**40%**)

D

* Reaction	Enzymes
Fructose 6-P ⇄ Fructose 1,6-BP	PFKP, PFKL, PFKM, PFKFB3, PFKFB4
2-Phosphoglycerate ⇄ PEP	ENO2, ENO1, ENO3
Pyruvate → Acetyl CoA	PDHA1, PDHB, PDHX, DLD
Succinate ⇄ Fumarate	SDHA, SDHAF1, SDHAF2, SDHAF4, SDHAP1

Legend: eIF5B-dependent; identified by TE analysis — eIF5B-dependent; identified by TE and protein output analyses

E **Hypoxia proteomics analysis**: Fold change (eIF5B deficient / replete)

		Protein output	Steady-state protein level
Hsp70	HSPE1 (Hsp10)	0.92	0.54
	HSPB1 (Hsp27)	0.98	0.89
	HSPA2	1.02	0.90
	HSPA4	1.44	0.91
	HSPA8	1.34	0.94
	HSPA14	2.08	5.58
Hsp90	HSP90AA1	1.09	1.03
	HSP90AB1	1.15	0.89
	HSPH1 (Hsp110)	2.03	1.57

F

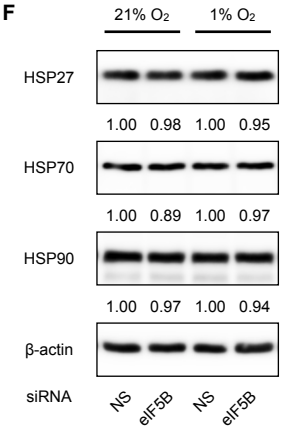

G

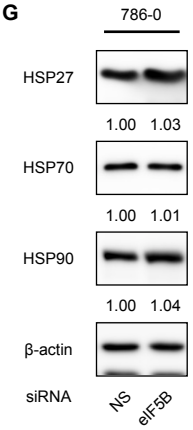

Figure S4. Related to Figure 4. (**A, B,** top panel) KEGG pathway enrichment analysis of eIF5B-dependent cellular systems. (**B,** bottom panel) Hexagon models are shown, depicting TE, steady-state RNA level, protein output, and steady-state protein level for each individual detected protein involved in amino acid synthesis and protein processing, cell adhesion, and endocytosis. Legend is shown in Figure 4B. **(C)** Distribution of eIF5B-dependent targets across the three hypoxia-responsive classes. **(D)** Full list of eIF5B-dependent enzymes and/or isoforms identified to participate in the specific central carbon metabolism pathways. **(E)** Change in protein output and steady-state protein levels for heat shock proteins in eIF5B depleted (eIF5B-specific siRNA) versus eIF5B replete (control non-silencing (NS) siRNA), hypoxic U87MG cells. Representative immunoblots of **(F)** normoxic and hypoxic U87MG cells and **(G)** normoxic 786-0 treated with NS or eIF5B-specific siRNAs.

Supplemental Experimental Procedures. Related to Experimental Procedures.

Mass spectrometry analysis. Samples were re-suspended in 100 uL of 50 mM NH_4HCO_3 (pH 8.3), 8 M Urea, and DTT was added to reduce cysteines at a final concentration of 10 mM. Cysteines were reduced at 60°C for 1 hour. Sample was cooled to room temperature and iodoacetamide was added to a final volume of 20 mM. Samples were incubated at room temperature in the dark for 30 min. Samples were then acetone precipitated overnight, and protein precipitates were centrifuged at 23,000 g for 15 min. Precipitates were re-suspended in 50 uL of NH_4HCO_3 (pH 8.3), and MS grade Trypsin/LysC (Promega) was added to a final protease:protein ratio of 1:50 and samples were digested overnight at 37 ^{0}C. Samples were lyophilized and re-suspended in 0.1% trifluoroacetic acid (TFA). Peptides were fractionated using the Pierce High pH Reverse Phase Peptide Fractionation Kit (Pierce), following the manufacturer's instructions. Each sample was fractionated into 8 high pH fractions.

Fractionated peptides were lyophilized, and lyophilized peptide mixtures were dissolved in 0.1% formic acid and loaded onto a 75 μm x 2 cm PepMap 100 Easy-Spray pre-column filled with 3 μm C18 beads (Thermo Fisher Scientific) followed by an in-line 75 μm x 50 cm PepMap RSLC EASY-Spray column filled with 2 μm C18 beads (Thermo Fisher Scientific) at a pressure of 700 BAR. Peptides were eluted over 120 to 240 min at a rate of 250 nl/min using a 0 to 35% acetonitrile gradient in 0.1 % formic acid. For ribosome density fractionated samples, "free" fractions were eluted over 120 min each, while "40/60/80S" and "polysome" fractions were eluted over 180 each. eIF5B-depleted and control samples were eluted over 240 min each. Peptides were introduced by nanoelectrospray into an LTQ-Orbitrap Elite hybrid mass spectrometer (Thermo-Fisher) outfitted with a nanospray source and EASY-nLC split-free nano-LC system (Thermo Fisher Scientific). The instrument method consisted of one MS full scan (400–1500 m/z) in the Orbitrap mass analyzer, an automatic gain control target of 1e6 with a maximum ion injection of 200 ms, one microscan, and a resolution of 240,000. Ten data-dependent MS/MS scans were performed in the linear ion trap using the ten most intense ions at a normalized collision energy of 35. The MS and MS/MS scans were obtained in parallel fashion. In MS/MS mode automatic gain control targets were 1e5 with a maximum ion injection time of 50 ms. A minimum ion intensity of 5000 was required to trigger an MS/MS spectrum. Dynamic exclusion was applied using a maximum exclusion list of 500 with one repeat count with a repeat duration of 30 s and exclusion duration of 15 s.

Raw MS files acquired from the mass spectrometer were processed using PEAKS software (Bioinformatics Solutions Inc.). Data was loaded into the software program and data from each fraction was refined to merge scans within 2 min and 10.0 ppm. Spectra with PEAKS filter scores <0.5 were excluded. *De novo* sequencing and database searching was done using a precursor mass cutoff of 10.0 ppm and a fragment mass tolerance of 0.6 Da. Carbidomethylation of cysteine (+57.02 Da) residues was selected as a fixed modification while variable modifications included $^{13}C_6$-$^{15}N_2$ SILAC on K (8.01Da), $^{13}C_6$-$^{15}N_4$ SILAC on R (10.02), Oxidation of M (15.99). Label-free quantification was performed in PEAKS using SILAC labels. Data sets are available at the PRoteomics IDEntifications (PRIDE) database via ProteomeXchange, accession PXD006799.

RNA interference. Small interfering RNA (siRNA) pools (siGENOME siRNA, GE Dharmacon) were transfected at a final concentration of 50 nM using Effectene (Qiagen) for 48 hr.

Cell viability assays. Fluorescein diacetate (FDA) staining was used to assess cell viability. Briefly, cells were incubated in FDA (10 μg/ml) for 30 min at 37^0C with DAPI counterstaining, and visualized with fluorescence microscopy (excitation and emission wavelengths of 492 nm and 517 nm, respectively) after washing with PBS. In addition, cell viability measurements were performed using the RealTime-Glo MT Cell Viability Assay (Promega) at indicated time points over 48 hr on cells grown in the same well.

Global protein synthesis measurements. Global protein synthesis was measured by puromycin (Thermo Fisher Scientific) incorporation (1 μg/ml) for 20 min, followed by immunoblot analysis with an anti-puromycin antibody (see below).

Immunoblot. Immunoblots were performed using standard techniques using the following antibodies: β-actin (Thermo Fisher Scientific, MA5-15739), ATF4 (Cell Signaling Technology, 11815S), total eIF2α (Cell Signaling Technology, 5324), Ser51-phosphorylated eIF2α (Abcam, ab32157), eIF2A (Proteintech, 11233-1-AP), eIF2D (Proteintech, 12840-1-AP), eIF5B (Santa Cruz Biotechnology, sc-393564), GLUT1 (Novus Biologicals, NB110-39113), HIF-2α (Novus Biologicals, NB100-122), HSP27 (Cell Signaling Technology, 2402S), HSP70 (Santa Cruz Biotechnology, sc-66048), HSP90 (Cell Signaling Technology, 4877S), NDRG1 (Abcam, ab37897), P4HA1 (Novus

Biologicals, NB100-57852), and puromycin (EMD Millipore, MABE343). HRP-conjugated secondary antibodies (Santa Cruz Biotechnology) were used. Signals were detected by chemiluminescence (Pierce) using an Amersham Imager 600 (GE Healthcare Life Sciences) and analyzed in ImageJ (NIH).

RNA immunoprecipitation. eIF5B RNA immunoprecipitation (RIP) experiments were performed using the Imprint RNA Immunoprecipitation Kit (Sigma-Aldrich) according to the manufacturer's protocols. Whole cell lysates extracted with mild lysis buffer were incubated with an eIF5B/IF2-specific antibody (Bethyl Laboratories Inc., A301-744A) at 4 ^{0}C overnight. 200 µl of lysate and 7.5 µg of pre-bound antibodies were used for each RIP reaction.

Reverse transcription-quantitative polymerase chain reaction (RT-qPCR). First-strand cDNA synthesis was performed using the High-Capacity cDNA Reverse Transcription Kit (Thermo Fisher Scientific), according to the manufacturer's protocol. qRT-PCR was performed using the PowerUp SYBR Green Master Mix (Thermo Fisher Scientific) and a StepOnePlus Real-Time PCR System (Applied Biosystems, Thermo Fisher Scientific). All primer sequences are available upon request. Relative changes in expression were calculated using the comparative Ct ($\Delta\Delta$Ct) method.

RNA-sequencing and analysis. Equal volumes of relevant ribosome density fractionated fractions were combined to yield the "free", "40/60/80S", and "polysome" samples, respectively. Poly(A) RNA selection, library preparation, and RNA sequencing were performed by the Sylvester Comprehensive Cancer Center Oncogenomics Core Facility, using the KAPA Stranded mRNA-Seq Kit (KAPA Biosystems) and NextSeq 500 High Output Kit v2 (Illumina). Paired-end (2 x 75 bp) sequencing runs at a depth of >50 million reads were performed on the libraries using the NextSeq 500 system (Illumina).

Raw data pre-processing was performed by the Sylvester Comprehensive Cancer Center Biostatistics and Bioinformatics Core Facility. For differential expression analysis, raw paired-end read data in FASTQ format were assessed for quality with FastQC (v. 11.5, Babraham Bioinformatics). Trimmomatic (Bolger et al., 2014) (v. 0.32) was used to remove adapters, Illumina-platform specific sequences, and low quality leading and trailing bases.

STAR (Dobin et al., 2013) ((v. 2.5.0) was then utilized to map reads to the reference transcriptome (UCSC hg38 knownGene database). Results were then processed by SAMtools (Li et al., 2009) (v. 0.1.19) for assignment to genomic features using featureCounts (Liao et al., 2014) in the Subread package (Liao et al., 2013) (v. 1.5.0). Transcript quantification (Fragments Per Kilobase of transcript per Million mapped reads, FPKM) was performed with RSEM (Li and Dewey, 2011) (v. 1.2.31) with a reference transcriptome (gencode.v26.p10.h38). Following input adjustment, translation efficiency was calculated based on polysomal to monosomal FPKM ratio. Steady-state RNA (transcriptome) levels were calculated based on the sum of FPKM across all fractions. Data sets are available at the NCBI Sequence Read Archive (SRA) database, accession SRP110475.

Kyoto Encyclopedia of Genes and Genomes (KEGG) pathway enrichment analysis. KEGG analysis was performed using the Database for Annotation, Visualization, and Integrated Discovery (DAVID) bioinformatics resource (Huang da et al., 2009) (v. 6.8).

Supplemental References

Bolger, A.M., Lohse, M., and Usadel, B. (2014). Trimmomatic: a flexible trimmer for Illumina sequence data. Bioinformatics *30*, 2114-2120.

Dobin, A., Davis, C.A., Schlesinger, F., Drenkow, J., Zaleski, C., Jha, S., Batut, P., Chaisson, M., and Gingeras, T.R. (2013). STAR: ultrafast universal RNA-seq aligner. Bioinformatics *29*, 15-21.

Huang da, W., Sherman, B.T., and Lempicki, R.A. (2009). Systematic and integrative analysis of large gene lists using DAVID bioinformatics resources. Nat Protoc *4*, 44-57.

Li, B., and Dewey, C.N. (2011). RSEM: accurate transcript quantification from RNA-Seq data with or without a reference genome. BMC Bioinformatics *12*, 323.

Li, H., Handsaker, B., Wysoker, A., Fennell, T., Ruan, J., Homer, N., Marth, G., Abecasis, G., Durbin, R., and Genome Project Data Processing, S. (2009). The Sequence Alignment/Map format and SAMtools. Bioinformatics *25*, 2078-2079.

Liao, Y., Smyth, G.K., and Shi, W. (2013). The Subread aligner: fast, accurate and scalable read mapping by seed-and-vote. Nucleic Acids Res *41*, e108.

Liao, Y., Smyth, G.K., and Shi, W. (2014). featureCounts: an efficient general purpose program for assigning sequence reads to genomic features. Bioinformatics *30*, 923-930.